Journal of Power Sources 267 (2014) 673–681

Contents lists available at ScienceDirect

Journal of Power Sources

journal homepage: www.elsevier.com/locate/jpowsour

Anderson type polyoxomolybdate as cathode material of lithium battery and its reaction mechanism

Erfu Ni, Shinya Uematsu, Noriyuki Sonoyama*

Department of Materials Science and Engineering, Nagoya Institute of Technology, Gokiso-cyo, Showa-ku, Nagoya 466-8555, Japan

HIGHLIGHTS

- Anderson type polyoxomolybdate $Na_3[AlMo_6O_{24}H_6]$ (NAM) show high discharge capacity.
- 91.2% of initial discharge capacity for NAM was retained after 50 cycles.
- The molecular cluster ion is stable, in spite of rapid amorphization of crystal.

ARTICLE INFO

Article history:
Received 11 February 2014
Received in revised form
27 May 2014
Accepted 28 May 2014
Available online 7 June 2014

Keywords:
Anderson type polyoxomolybdate
Cathode material
Lithium battery
Molecular cluster ion

ABSTRACT

Anderson type polyoxomolybdate, $Na_3[AlMo_6O_{24}H_6]$ (NAM), was studied as the cathode material of lithium battery. Discharge capacity and cycle performance of NAM cathode largely depended on the mixing method of active material with conductive additive and the type of conductive additive. NAM ball-milled with ketjen black (KB) showed very high initial discharge capacity of 437 mAh g^{-1} and the most stable cycle performance with high capacity retention of 91.2% after 50 cycles. The results of *ex situ* XRD showed that the crystal structure changes of NAM was irreversible during the first discharge–charge process and changed to amorphous state completely after 5 cycles. *Ex situ* Raman spectra showed the structure of molecular cluster ion $[AlMo_6O_{24}H_6]^{3-}$ is stable during the discharge process. These data have demonstrated that the high discharge capacity and stable cycle performance of NAM originate in the improvement of the electric conductivity and the stable molecular cluster ion $[AlMo_6O_{24}H_6]^{3-}$ that is independent from the recoverability of its crystal structure.

1. Introduction

Lithium ion batteries have attracted much attention as energy storage devices for the next generation of electrical devices and vehicles. Currently, as the cathode materials for lithium ion batteries, the lithium intercalation materials, such as layered lithium transition metal oxides and lithium transition metal polyanions, which include lithium ion in their lattices, are used mainly. For these materials, the capacity and cycle stability are mainly determined by the recoverability of the crystal structure in the process of lithium extraction-insertion. For example, the phase of Li_xMO_2 (M = Co or Ni) with a layered rock salt structure changes with the extraction of lithium from hexagonal to monoclinic and then backs to hexagonal, with a different structure from the initial state. The recoverability of the initial hexagonal phase by insertion of lithium determines the useable limit of deintercalation to be $x = 0.5$ (monoclinic phase) [1–4].

Cluster materials have drawn attention as a new cathode material for lithium battery [5–8]. In previous papers, we indicated that molecular cluster ion electrodes are expected to show intermediate properties between lithium intercalation electrodes and organic radical electrodes [7,8]. Usually, cluster ions consist of several (or ten-odd) metal ions in a unit. They behave as a single molecule under dissolved conditions in solvents. In the solidification process, cluster ions form ionic crystals with some counter ions, while some of them become amorphous. These cluster ion materials are expected to show redox activity as an individual molecular cluster, not as a continuum [9]. Therefore, the capacity and cycling capability of the cluster materials are independent from the stability or recoverability of its crystal structure. This independence of properties from the crystal structure will enable deep discharge–charge and high capacity in the wide voltage window.

In the previous papers, we have focused on the polyoxometalates (POMs), molybdate $K_3[PMo_{12}O_{40}]$ (KPM) with Keggin

* Corresponding author. Tel./fax: +81 52 735 7243.
E-mail address: sonoyama@nitech.ac.jp (N. Sonoyama).

http://dx.doi.org/10.1016/j.jpowsour.2014.05.141
0378-7753/

type structure [7] and vanadate $(KH)_9[PV_{14}O_{42}]$ (KPV) with bi-capped Keggin type structure [8], as cathode materials for lithium battery. Both KPM and KPV showed discharge–charge performance with a capacity over 200 mAh g^{-1} in the voltage range of 1.5–4.2 V. However, the KPM showed poor cycle stability, which should be due to the unstable structure of cluster ion unit $[PMo_{12}O_{40}]^{3-}$ in the reduced state [10]. On the other hand, the KPV exhibited excellent cycling capability with capacity retention of 95% after 50 discharge–charge cycles owing to its comparatively stable structure of cluster ion unit $[PV_{14}O_{42}]^{9-}$. From these results, it is suggested that the stable structure of cluster ion unit during redox reaction is very important for improving the cycle stability of POMs as cathode materials, and it is expected that POMs with further stability will show higher battery performance, e.g. high capacity with deep discharge and high cycle stability.

In this study, we have selected an Anderson type polyoxomolybdate, $Na_3[AlMo_6O_{24}H_6]$ (NAM), as the new cathode material for lithium battery with high capacity and stability. Fig. 1 shows the structure of Anderson type polyoxomolybdate and the crystal structure of NAM. In the Anderson type structure, all MoO_6 octahedra are directly connecting with central Al^{3+} ion with the covalent bonding, and all the metal atoms are in a common plane. This structure is expected to be stable during the redox owing to the strong covalent binding. In addition, the crystal structure of NAM has three-dimensional framework in which lithium ions can diffuse. The theoretical capacity of NAM is assumed to be 455 mAh g^{-1} (1C), corresponding to the insertion of 18 Li into the structure, which requires 6 redox couples of Mo^{6+}/Mo^{3+} in one cluster ion unit $[AlMo_6O_{24}H_6]^{3-}$. However, POMs tend to show low electric conductivity. The poor performance of the cathode materials originated from its low electric conductivity can be improved by mixing with conductive additive carbon with high electric conductivity such as ketjen black (KB), that has been demonstrated in the case of $LiFePO_4$ and $LiMnPO_4$ [11,12]. To improve the low electric conductivity of POMs, NAM was mixed with acetylene black (AB) or KB by hand-grinding and ball-milling, and the electrochemical properties of NAM in each mixing system were examined. The crystal structure changes of NAM and the structural stability of molecular cluster ion $[AlMo_6O_{24}H_6]^{3-}$ during the discharge–charge process were observed by *ex situ* XRD and *ex situ* Raman measurements, respectively, and reaction mechanism of Anderson type POM and lithium ions during discharge–charge was discussed.

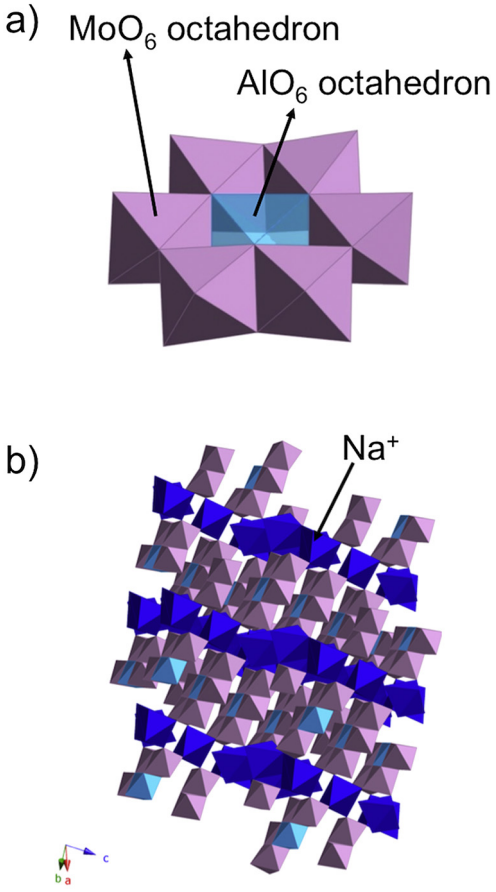

Fig. 1. a) Structure of Anderson type polyoxomolybdate; b) crystal structure of $Na_3[AlMo_6O_{24}H_6]$.

2. Experimental

We have modified the reported synthesis method of NAM [13]. The synthesis procedure is summarized as follows. 3.5 g $Na_2MoO_4 \cdot 2H_2O$ (Kishida, GR) was added to a solution of 0.829 g $AlCl_3$ (Kishida, GR) in 25 ml of distilled water with stirring. The pH of the solution was adjusted to 1.8 by dropwise addition of 35% hydrochloric acid (Kishida, GR). Thereafter the clear solution was evaporated slowly at 40 °C with stirring. The white crystal precipitate was filtered, washed with 2:1 v/v acetone-distilled water followed with acetone. To remove the water in crystal, the obtained powders were dried at 80 °C for 12 h.

The crystal structure of NAM powder was identified by X-ray diffraction (XRD) measurement using a powder X-ray diffractometer (Rigaku RAD-C) with Cu Kα (40 kV, 40 mA) radiation. The diffraction data were collected from 10 to 90° in 2θ. Morphology of NAM particles was obtained by a scanning electron microscope (HITACHI S-4800). The crystal structure of as-prepared NAM was refined by the Rietveld analysis using the computer program RIETAN-2000 [14,15]. FT–IR spectra were collected with a JASCO-410 spectrometer in the range of 500–1200 cm^{-1}. Pellets for FT–IR measurement were prepared by grinding and pressing samples with dried KBr powder (Kishida infrared spectra grade). Raman spectra were recorded with a Laser Raman Spectrometer (JASCO NRS-3300) in the energy range 350–1050 cm^{-1} with the probe light of Raman scattering, DPSS laser at a wavelength of 532 nm was used. The electrochemical properties of NAM electrodes were tested at 25 °C by using CR-2032 coin cells, which were assembled in an argon filled glovebox using metallic lithium (Honjyo metal) as anode, and 1 M $LiPF_6$ in mixture of ethylene carbonate (EC) and diethyl carbonate (DEC) (3:7, v/v: Kishida battery grade) as the electrolyte solution. The cathodes were prepared either by hand-grinding NAM with AB or KB, or dry mechanical milling NAM with AB or KB with planetary ball mill (Fritsch P-7) under air. The following conditions were used for the ball-milling. The weight rations of NAM:AB(KB) are 1:2, 1:1, 2:1 or 3:1, respectively; milling media: three balls with 10.5 mm in diameter each and sixteen smaller balls with 5 mm in diameter each; volume of milling vessel: 45 ml; milling media and vessel material: zirconium dioxide; milling speed: 500 rpm; milling time: 1 h. Unless specifically noted otherwise, all of the cathodes consisted of NAM active material, AB or KB conductive additives and PTFE binder in the weight ratio of 32:64:4. The discharge–charge properties of the cells were recorded on a battery tester (Interface model OZO-A19) between 1.5 and 4.2 V (vs. Li/Li^+) at the current density of 17 mA g^{-1} (0.04C), otherwise noted. Solartron analytic instruments consisting of a frequency-response analyzer (Solartron 1255) and a potentiostat (Solartron 1280) were used to acquire electrochemical impedance spectroscopy (EIS) in the frequency range 10^6–10^{-2} Hz with an amplitude of 10 mV.

The structural change of NAM during discharge–charge process was investigated by *ex situ* XRD and *ex situ* Raman measurements under Ar atmosphere. After discharge and charge of the cells, the cathode materials were removed from separable cells (Hosen HS cell) in Ar atmosphere glovebox. After rinsing with dimethyl carbonate (Kishida battery grade) and drying in glovebox, *ex situ* XRD measurements were performed by enclosing the cathode sample in lab made cell equipped with Mylar film window. *Ex situ* Raman spectra were recorded by covering the cathode sample closely with a glass sheet with thickness of 0.15 mm and sealing the edges of glasses with vinyl acetate resin.

3. Results and discussion

3.1. Crystal and molecular structures

The XRD pattern of as-prepared NAM is shown in Fig. 2. All of the reflections are consistent with those of NAM in ICSD No. 281185. The crystal structure was refined by the Rietveld analysis using the model with the space group *P*-1. The result of refinement is shown in the Supplementary data. The Rietveld refined lattice parameters for as-prepared NAM in this study are $a = 12.13339$ Å, $b = 13.14839$ Å, $c = 14.25429$ Å, $\alpha = 80.7819°$, $\beta = 74.6745°$, $\gamma = 68.6884°$, those are a little different from those of the reported NAM [13]. It is noted that the intensity ratios of the as-prepared NAM around $2\theta = 10–20°$ do not match well the ICSD pattern. This would be caused by the difference in the orientation of powders, because the conditions for the crystal growth in our work are different from that of the reported one in ICSD. The XRD pattern of NAM after drying treatment was different from NAM before drying, which would be caused by the removal of crystal water in NAM. To confirm the structural stability of molecular cluster ion $[AlMo_6O_{24}H_6]^{3-}$ after drying treatment, the FT–IR spectra were measured. As can be seen in Fig. 3, the characteristic peaks of dried NAM in the wavenumber range of 500–1200 cm^{-1} agreed with those of as-prepared NAM before drying, indicating that the structure of the molecular cluster ion was maintained even after the crystal structure change of NAM by drying treatment. Fig. 4 shows the morphology of as-prepared NAM observed by SEM at different magnifications, the surface images revealed that the powders of NAM were aggregates of shapeless particulates from nanosize to microsize.

Fig. 5 shows the XRD patterns of NAM after ball-milling with AB or KB. Most of the reflections in the $41° < 2\theta < 90°$ almost disappeared for the ball-milled samples, while the reflections in the $10° < 2\theta < 41°$ became weaker and broader compared with the sample without ball-milling, demonstrating that the crystallinity of the ball-milled samples decreased. In addition, the positions of reflections for the ball-milled samples shifted to the lower angles (as illustrated in the inset of Fig. 5). This indicates that a slight expansion of lattice by ball-milling with the conductive additives. This result is consistent with the variability of the NAM crystal by drying. Fig. 6a and b shows the SEM images of NAM mixed with AB by hand-grinding and ball-milling, respectively. The particle size of NAM was not decreased significantly by mechanical ball-milling.

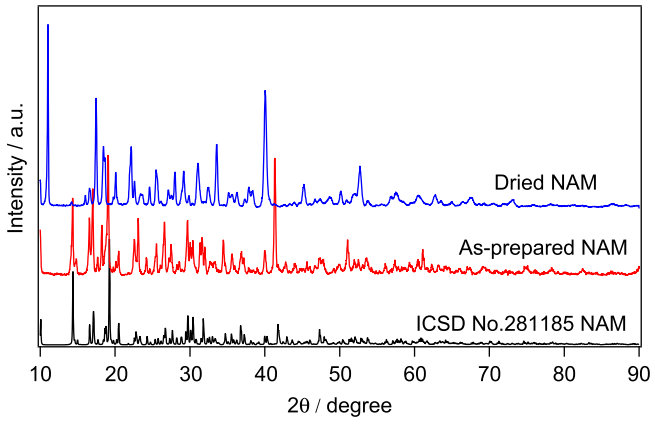

Fig. 2. XRD patterns of ICSD No. 281185, as-prepared and dried NAM.

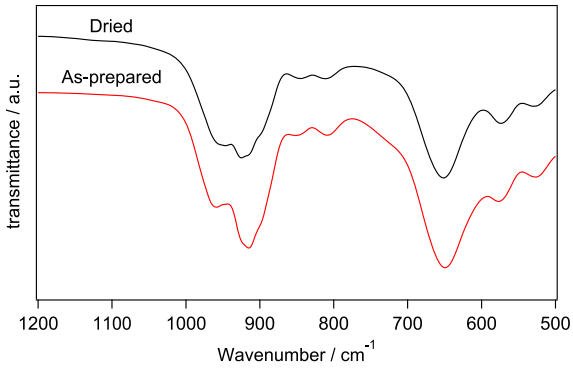

Fig. 3. FT–IR spectra of as-prepared and dried NAM.

3.2. Electrochemical properties of NAM

Fig. 7a shows discharge–charge curves in the first and second cycles of NAM mixed with AB by hand-grind (NAM hand AB), with AB by ball-mill (NAM ball-mill AB), with KB by hand-grind (NAM hand KB), with KB by ball-mill (NAM ball-mill KB), respectively. The NAM hand AB showed large flat discharge voltage plateau between 1.8 and 2.0 V and its initial discharge capacity reached 278 mAh g^{-1}. In the subsequent charge process, this system showed steep polarization when recharged up to the voltage higher than 2.0 V, and a very small voltage plateau was obtained around 3.0 V. This polarization would be due to the difficulty in extracting the lithium ions from NAM, and caused a very large irreversible capacity loss of 152 mAh g^{-1} after the first charge. Interestingly, this polarization was decreased significantly by ball-milling NAM with AB. Initial discharge capacity of 287 mAh g^{-1} was obtained by NAM ball-mill AB, which is higher than that of NAM hand AB, and the irreversible capacity loss after the first charge was decreased to 61 mAh g^{-1}, which is much lower than that of NAM hand AB. It is noted that the average discharge voltage of NAM ball-mill AB was also improved to 2.11 V compared with that of 1.92 V for NAM hand AB. These results suggest that, as was expected, low electric conductivity of NAM caused high polarization to the NAM hand AB system. It is expected that by mixing NAM with conductive additive with higher electric conductivity in comparison with AB conductive additive, much higher discharge capacity will be obtained, due to the multi-electron redox, that we have reported to occur in the discharge–charge process of POMs [7,8]. As conductive additive, AB shows ball-like particle with specific surface area of 76 m^2 g^{-1}, while KB has porous and chain-like structure, giving rise to higher specific surface area (800 m^2 g^{-1}) and much more conductive paths than AB [16]. Therefore, KB was chosen as the conductive additive because it has higher electric conductivity than AB. As was above expected, much higher initial discharge capacity of 421 mAh g^{-1} was obtained by hand-grinding NAM with KB. The polarization in the charge process for NAM hand KB was further decreased in comparison with that of NAM hand AB and NAM ball-mill AB. However, an irreversible charge capacity of 77 mAh g^{-1} was still obtained after the first cycle. As mentioned above, the mechanical ball-milling has shown effectiveness in improving the reversible

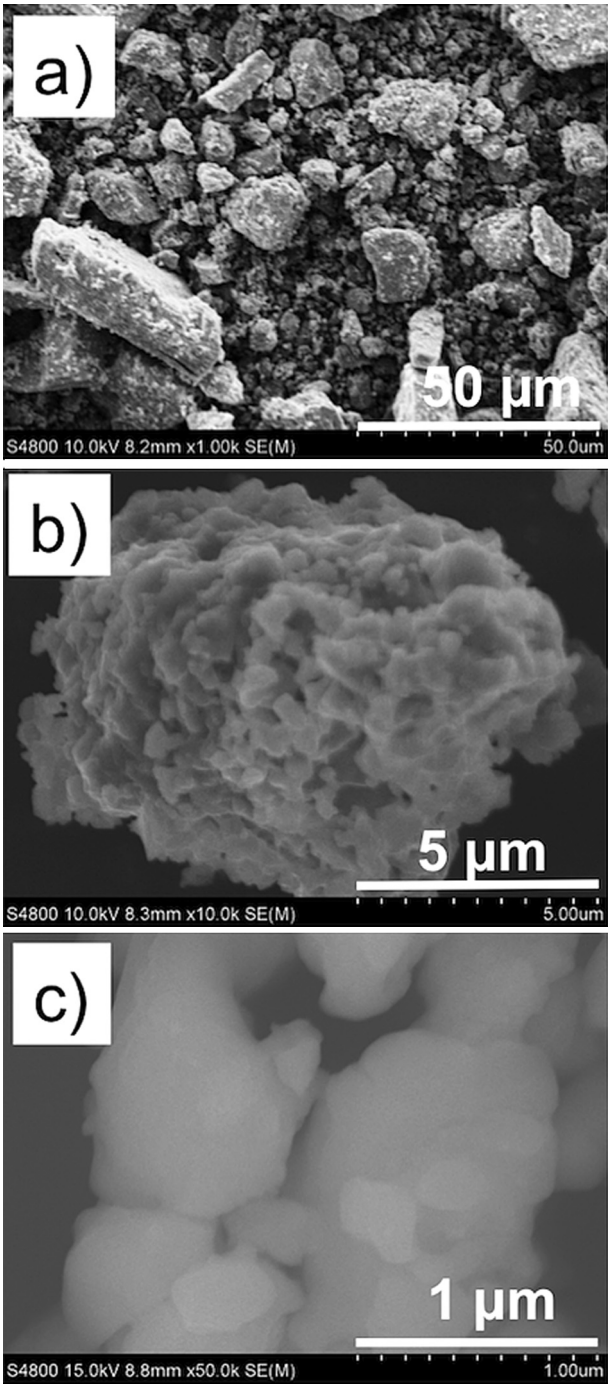

Fig. 4. The morphology of as-prepared NAM observed at different magnifications: a) ×1 k; b) ×10 k; c) ×50 k.

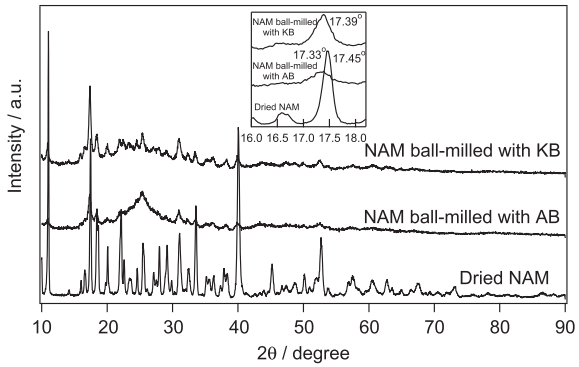

Fig. 5. XRD patterns of NAM after ball-milling with AB or KB.

capacity after the first charge for the system of NAM ball-mill AB. In order to reduce the irreversible charge capacity for NAM mixed with KB, the mechanical ball-milling NAM with KB was carried out. In comparison with NAM hand KB, the initial discharge capacity was improved to 437 mAh g^{-1}, and almost reversible charge capacity of 429 mAh g^{-1} was obtained after the first cycle for NAM ball-mill KB. It is noteworthy that all of the systems showed almost reversible discharge and charge capacities in the second cycle.

Fig. 7b shows the cycle performance of NAM in various mixing systems after 50 cycles. The NAM hand AB showed steep capacity loss after the first cycle until the 10th cycle. Thereafter capacity faded continuously and discharge capacity of only 49 mAh g^{-1} was obtained after 50 cycles. On the other hand, NAM ball-mill AB showed higher discharge capacity than NAM hand AB, though the capacity continued decreasing gradually with cycling. After 50 cycles, capacity of 132 mAh g^{-1} was retained for NAM ball-mill AB. Similarly to NAM hand AB, NAM hand KB also showed notable capacity loss from the first cycle to the 6th cycle, but the capacity increased slightly with increase of cycle number to the 20th cycle, thereafter cycle performance tended to be stable. When NAM was inhomogeneously mixed with KB with large specific surface area by hand-grinding, it would take more time for the infiltration of electrolyte into the whole electrode. With the increase of cycling, the active material NAM was gradually activated due to the more and more electrolyte infiltrated into the electrode, resulting in the gradual increase of capacity. After 50 cycles, capacity of 299 mAh g^{-1} was obtained for NAM hand KB. It should be noted that NAM ball-mill KB showed very stable cycle performance with long-term cycling, capacity of 399 mAh g^{-1} corresponding to the capacity retention of 91.2% was obtained after 50 cycles.

To analyze the effect of the mechanical ball-milling and the type of conductive additive on the cycle performance of NAM, EIS measurements were carried out for the various mixing systems after 1 cycle and 20 cycles, the respective Nyquist plots are shown in Fig. 8. It can be seen that all of the Nyquist plots consist of one semicircle in the high-frequency range and a linear part in the low-frequency range. Nevertheless, the lines in the spectra of NAN hand AB are almost vertical to the Z′-axis (Fig. 8a), which correspond to the capacitive reactance instead of the solid-state diffusion of lithium ions (Warburg diffusion) in the cathode bulk material [17]. The vertical lines changed to the slope lines by mechanical ball-milling NAM with AB (Fig. 8b), indicating that the capacitive effect was substituted for the diffusion of lithium ions in the cathode. Therefore, as illustrated in Fig. 6a, the NAM hand AB showed the very large irreversible capacity in the first charge process, while the lower irreversible capacity was obtained for NAM ball-mill AB.

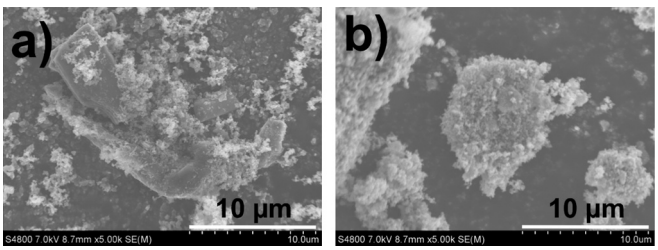

Fig. 6. Low magnification SEM images of NAM mixed with AB a) by hand-grinding and b) by ball-milling.

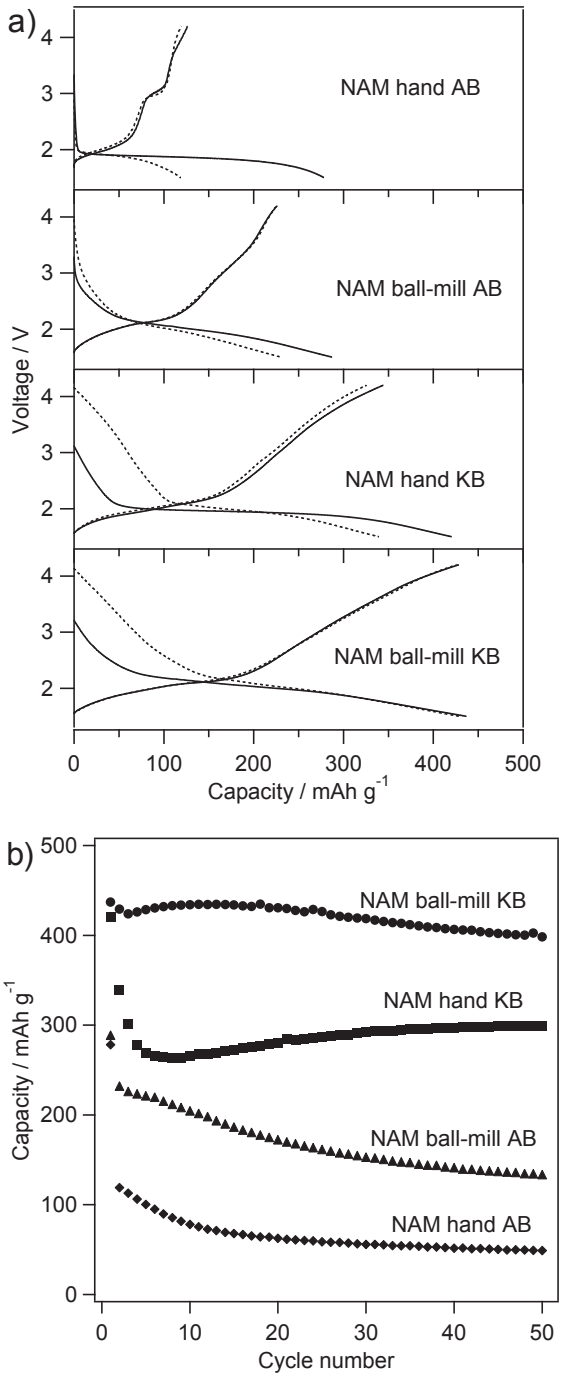

Fig. 7. a) The first two discharge–charge cycle curves (solid lines: 1st cycle, dash lines: 2nd cycle) and b) cycle performance of the different systems (C rate: 0.04C).

Fig. 9 shows the high magnification SEM images for NAM before (Fig. 9a) and after mixing with AB or KB by hand-grinding or ball-milling (Fig. 9b–e). It can be seen the particle surface was covered well with conductive additive after mechanical ball-milling. Fig. 10a and b shows the SEM images and the elemental distribution maps by EDS of NAM hand AB and NAM ball-mill AB, respectively. It can be seen that ground NAM particles and AB were mixed homogeneously in the cathode active material by ball-milling (Fig. 10b), whereas micrometer size NAM blocks presented in NAM hand AB active material (Fig. 10a). This result further indicates that the improved electrochemical property for NAM with ball-mill treatment should be ascribed to the higher contact surface

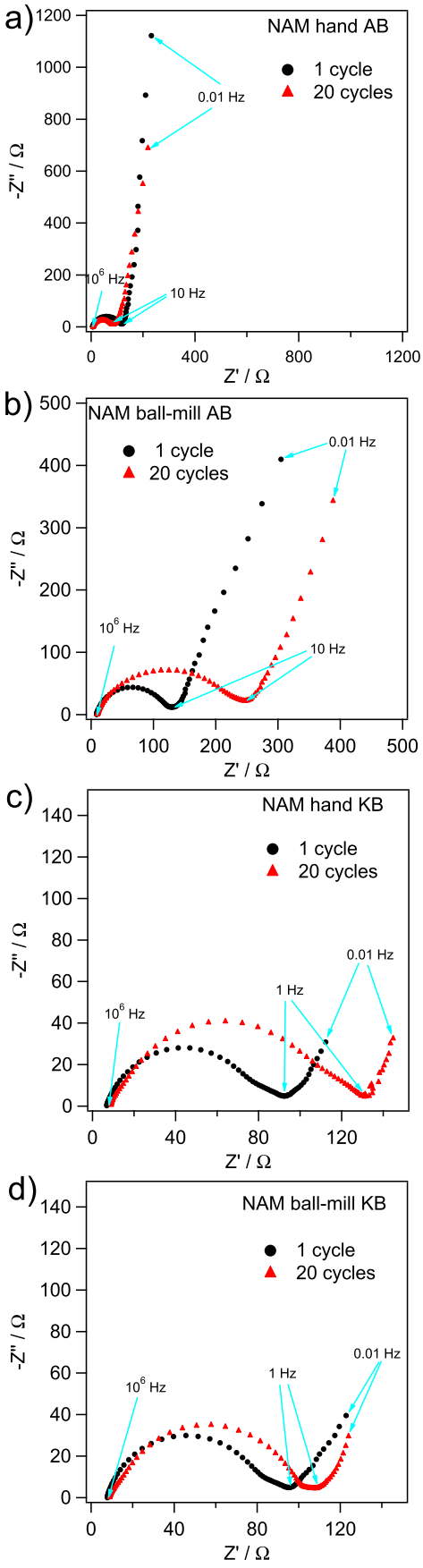

Fig. 8. Nyquist plots of a) NAM mixed with AB by hand-grinding, b) NAM mixed with AB by ball-milling, c) NAM mixed with KB by hand-grinding and d) NAM mixed with KB by ball-milling recorded after 1 cycle and after 20 cycles (C rate: 0.04C).

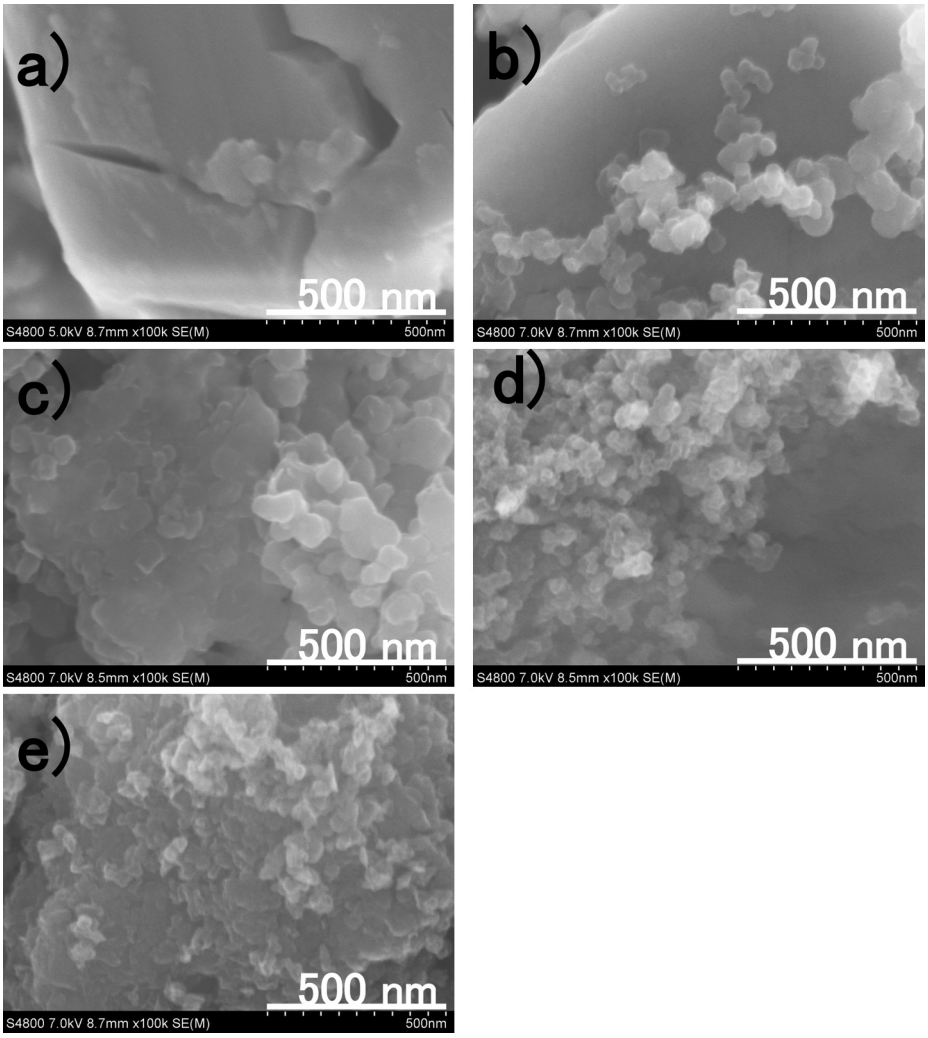

Fig. 9. High magnification SEM images of NAM before a) and after b) mixing with AB by hand-grinding, c) NAM mixed with AB by ball-milling, d) NAM mixed with KB by hand-grinding and e) NAM mixed with KB by ball-milling.

area between conductive additives and NAM particles, which improved the electric conductivity, facilitating the lithium diffusion in the electrode. This result is consistent with the reduced charge transfer resistance by the mechanical ball-milling (Fig. 8).

Although the electric conductivity of NAM was improved by mechanical ball-milling NAM with AB, due to the intrinsic low electric conductivity of AB, there was still large resistance for the charge-transfer during the discharge−-charge process. As illustrated in Fig. 8b, after 20 cycles, the charge-transfer resistance of NAM ball-mill AB increased largely, which should be responsible for the gradual capacity loss with the increase of cycle number. On the other hand, by changing the conductive additive from AB to KB, NAM hand KB showed lower charge-transfer resistance (Fig. 8c) than NAM ball-mill AB (Fig. 8b), indicating that the electric conductivity of NAM could be further improved by mixing with KB conductive additive. Nevertheless, NAM hand KB also showed increase in the charge-transfer resistance after 20 cycles (Fig. 8c), which should be caused by the inhomogenous mixing of NAM and KB by hand-grinding, as shown in Fig. 10a. The charge-transfer resistance of NAM ball-mill KB hardly changed after 20 cycles (Fig. 8d) compared to NAM hand KB (Fig. 8c), indicating the electric conductivity of NAM was greatly improved by ball-milling NAM with KB. This would be the reason that NAM ball-mill KB not only showed the highest discharge capacity but also the most stable cycle performance with long-term cycling compared to the others systems. To further confirm that NAM ball-milled with KB could significantly enhance the electric conductivity, resulting in improvement of electrochemical properties, the rate capability at higher C rate was examined, as shown in Fig. 11. NAM ball-mill KB showed much better rate capability than NAM hand KB.

The high carbon loading of the cathode decreases the energy density of the cell. The relationship between the loading KB weight, that effectively improved the electrochemical property of NAM, and the cycle performance of NAM was investigated. The cycle performance of the cathodes consisting different weight ratios of NAM:KB:PTFE by hand-grinding or ball-milling NAM with KB is shown in Fig. 12. The discharge capacity of NAM deceased as the KB loading was decreased. However, in comparison with NAM hand KB, NAM ball-mill KB still showed relatively stable cycle performance after the first cycle and much higher discharge capacity was retained after 50 cycles. For NAM ball-mill KB, the system NAM:KB:PTFE = 64:32:4 showed similar cycle stability to NAM:KB:PTFE = 48:48:4 system and held about 240 mAh g^{-1} after 50 cycles. For the system of NAM:KB:PTFE = 72:24:4, the capacity steeply decreased with the increase of cycle number and capacity faded to 134 mAh g^{-1} after 50 cycles. This result indicates that low amount of the conductive additive was still insufficient to cover the

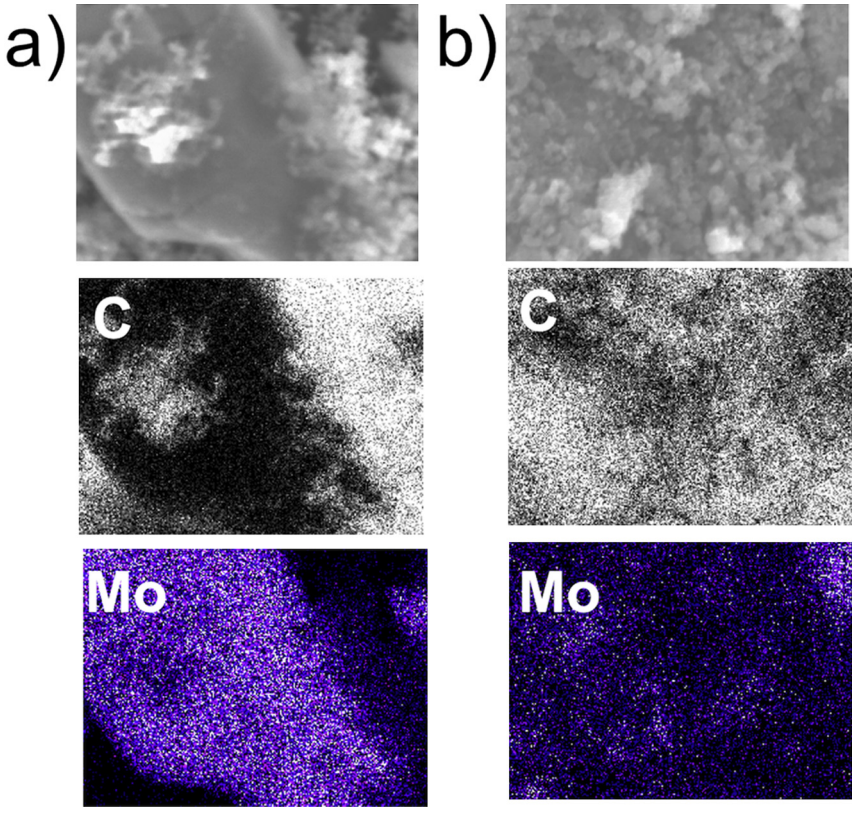

Fig. 10. SEM images and elemental distribution maps by EDS for a) NAM mixed with AB by hand-grinding and b) NAM mixed with AB by ball-milling.

surface of all NAM particles, leading to the low discharge capacity and poor cycle performance.

3.3. Reaction mechanism

In the investigation of POMs as the cathode materials of lithium battery, the reaction mechanism during discharge–charge process is very important, because POMs have intermediate property of the intercalation materials and molecular materials [7,8], and its properties will depend on the reaction mechanism. To investigate the discharge–charge reaction mechanism, the change in the crystal structure of NAM during the electrochemical reaction was probed by the *ex situ* XRD measurements. Fig. 13 shows the *ex situ* XRD patterns recorded at different voltages in the initial discharge process, after the first cycle and after 5 cycles. The XRD pattern of NAM before discharge was also plotted for comparison. It is clearly seen that the XRD pattern after discharging to 2.5 V was almost consistent with that of NAM before discharge, but the intensities of the reflections became weaker, and the positions of reflections shifted to the lower angle (as illustrated in the inset of Fig. 13). This indicates that the crystallinity of NAM decreased and its lattice expanded with the insertion of lithium ions. The XRD pattern did not show drastic changes when discharged to 2.0 V, indicating the crystal structure of NAM should be still maintained by the further insertion of lithium ions. Upon further discharging to 1.95 V, the reflections became much weaker and broader, and some reflections disappeared. Almost all of the reflections disappeared (except the

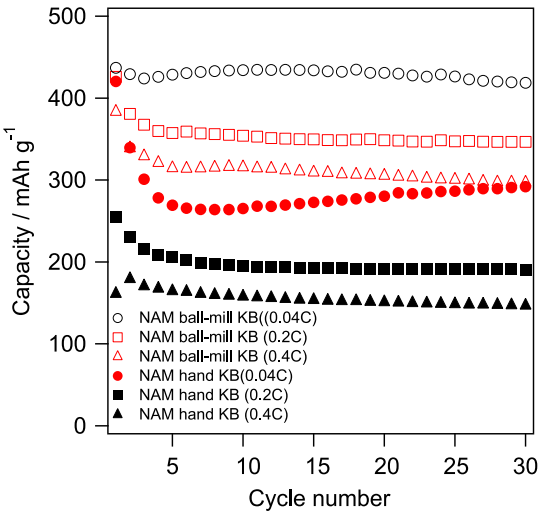

Fig. 11. Rate capability of NAM mixed with KB by hand-grinding and ball-milling.

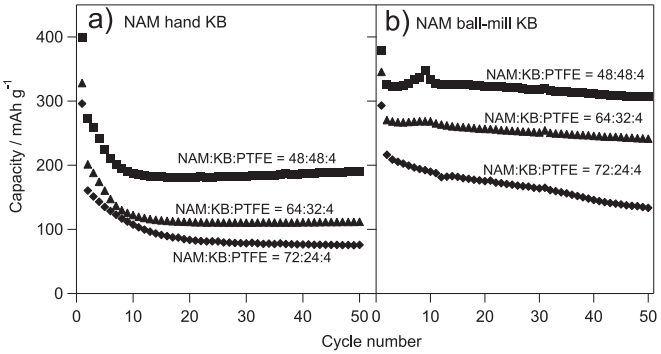

Fig. 12. Effect of the cathodes consisting of different weight ratios of NAM:KB:PTFE on the cycle performance of a) NAM mixed with KB by hand-grinding and b) NAM mixed with KB by ball-milling.

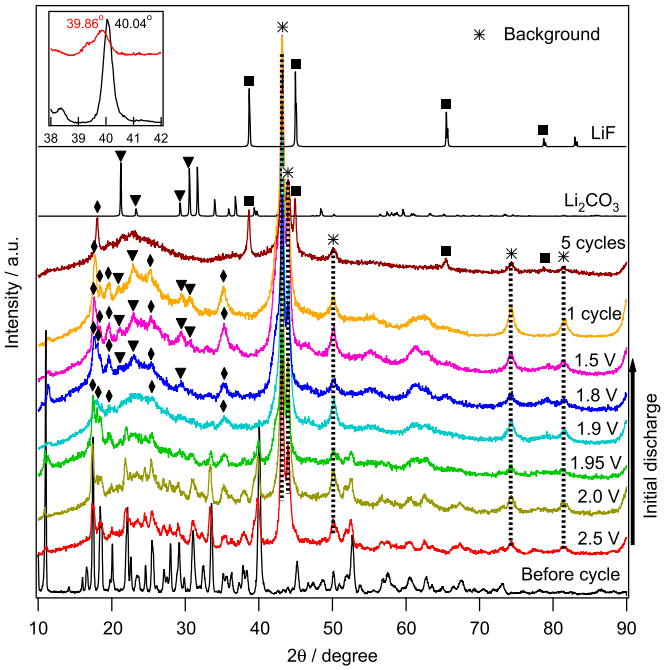

Fig. 13. *Ex situ* XRD patterns of NAM recorded at different voltages during the first discharge, after 1 cycle and after 5 cycles (peaks marked with * at $2\theta = 43.12°$, 43.96°, 49.99°, 74.2° and 81.44° are the backgrounds originated from the metal substrate; ⋄: reflections of NAM; ▼: reflections of Li_2CO_3; ■: reflections of LiF).

several reflections marked with ◆) when discharged to 1.9 V, indicating the crystal of NAM began to become amorphous. Upon further discharging from 1.8 V to the end of discharge at 1.5 V, the residual reflections of NAM did not change so much, but some new reflections (the positions marked with ▼) corresponding to the phase of Li_2CO_3 appeared. Li_2CO_3 should be arisen from the decomposition of electrolyte due to the deep discharge of NAM with the catalysis of POMs. In the following recharge process (after one cycle), Li_2CO_3 was still included in the cathode, while other reflections of NAM except the marked residual peaks did not appear again, indicating that the crystal structure of NAM was irreversible during the first discharge–charge process. After 5 cycles, all of the reflections of NAM except the main peak around 18° disappeared, indicating that the crystal structure changed to amorphous, and the decomposed product (Li_2CO_3) of electrolyte finally converted to LiF (reflections marked with ■).

To confirm the structural stability of the molecular cluster ion $[AlMo_6O_{24}H_6]^{3-}$ during the discharge–charge process, *ex situ* Raman spectra of NAM initially discharged to different voltages are plotted in Fig. 14. For NAM sample before cycle, the peaks at 971 cm^{-1} and 905 cm^{-1} were obtained, those are assigned to the vibrations of Mo–O bonds [13,18–20]. They shifted to lower wavenumbers with the insertion of lithium into the structure. The shift of Mo–O vibration to lower wavenumber corresponds to the decrease in electrostatic interaction with the reduction of molybdenum ion. The results of *ex situ* Raman spectra indicate that the structure of cluster ion unit $[AlMo_6O_{24}H_6]^{3-}$ is stable during the discharge process, even though the crystal structure of NAM becomes amorphous irreversibly.

On the basis of obtained data shown above, the schematic image of speculated discharge–charge mechanism for NAM is shown in Fig. 15. As we reported previously, $(KH)_9[PV_{14}O_{42}]$ (KPV) becomes amorphous after the first discharge and shows irreversibility of crystal structure change in the following charge process, but the molecular cluster ion unit $[PV_{14}O_{42}]^{9-}$ is still stable and continues to react with lithium reversibly [8]. NAM also shows the similar

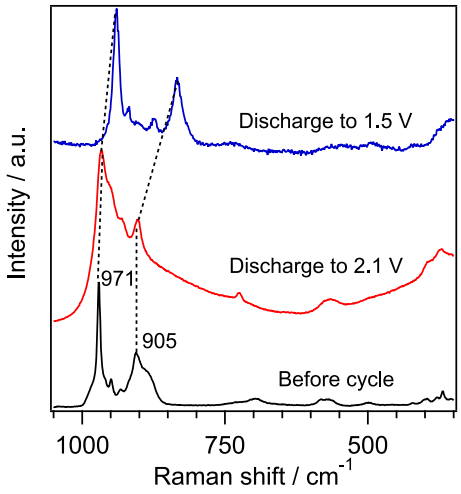

Fig. 14. *Ex situ* Raman spectra of NAM recorded at different voltages during the first discharge.

crystal structure change during the discharge–charge process. NAM crystal begins to become amorphous gradually during the initial discharge process. However, the molecular cluster ion $[AlMo_6O_{24}H_6]^{3-}$ is stable as was confirmed by the *ex situ* Raman spectra. In the following discharge–charge cycles, NAM changes to amorphous state completely, and the $[AlMo_6O_{24}H_6]^{3-}$ reacts with lithium ion reversibly as molecular cluster ion. Different from the conventional lithium intercalation materials in which the amount of lithium usable for extraction-insertion mainly depends on the recoverability of crystal structure, the insertion-extraction of lithium in NAM can continuously proceed in the amorphous structure upon the discharge–charge cycling. The high reversible discharge–charge capacity and good cycle stability of NAM would be ascribed to the reversible reaction of stable cluster ion unit $[AlMo_6O_{24}H_6]^{3-}$ with lithium ion in the deep discharge–charge process.

4. Conclusions

Anderson type polyoxomolybdate NAM was examined as the cathode material of lithium battery. The discharge capacity and

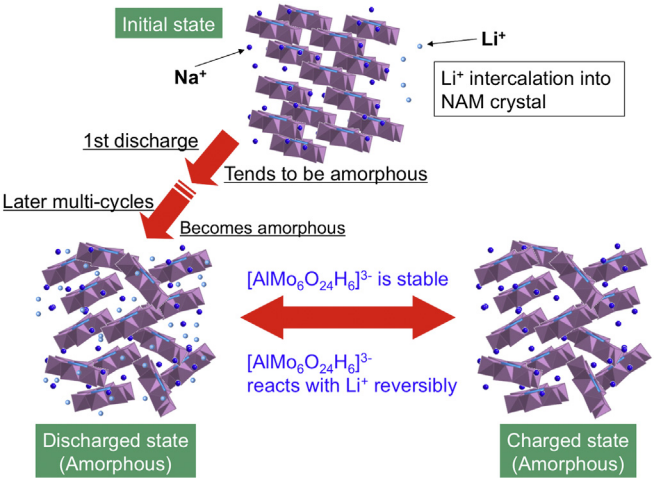

Fig. 15. The schematic image of reaction mechanism for NAM during the discharge–charge process.

cycle performance were improved by ball-milling NAM with AB or adding KB as conductive additive. Even though the crystal structure of NAM became amorphous by discharge–charge process, the molecular cluster ion $[AlMo_6O_{24}H_6]^{3-}$ was stable during the discharge–charge process; this means the electrochemical activity of NAM as a cathode material of lithium battery was not dependent on the recoverability of the crystal structure but on the stability of the molecular cluster ion. Based on our results in this study, we suggest that the stability of the molecular cluster ion unit is very important factor for using the molecular cluster ion compounds as the cathode materials of lithium battery.

Acknowledgments

This work was financially supported by NEDO (New Energy and Industrial Technology Development Organization) Li-EAD project. The authors would like to thank Prof. Imanishi at Mie University for the SEM measurements.

Appendix A. Supplementary data

Supplementary data related to this article can be found at http://dx.doi.org/10.1016/j.jpowsour.2014.05.141.

References

[1] T. Ohzuku, A. Ueda, J. Electrochem. Soc. 141 (1994) 2972–2977.
[2] X.Q. Yang, X. Sun, J. McBreen, Electrochem. Commun. 2 (2000) 100–103.
[3] J.N. Reimers, J.R. Dahn, J. Electrochem. Soc. 139 (1992) 2091–2097.
[4] B.L. Ellis, K.T. Lee, L.F. Nazar, Chem. Mater. 22 (2010) 691–714.
[5] H. Yoshikawa, C. Kazama, K. Awaga, M. Satoh, J. Wada, Chem. Commun. 30 (2007) 3169–3170.
[6] H. Yoshikawa, S. Hamanaka, Y. Miyoshi, Y. Kondo, S. Shigematsu, N. Akutagawa, M. Sato, T. Yokoyama, K. Awaga, Inorg. Chem. 48 (2009) 9057–9059.
[7] N. Sonoyama, Y. Suganuma, T. Kume, Z. Quan, J. Power Sources 196 (2011) 6822–6827.
[8] S. Uematsu, Z. Quan, Y. Suganuma, N. Sonoyama, J. Power Sources 217 (2012) 13–20.
[9] M.T. Pope, Y. Jeannin, M. Fournier, Heteropoly and Isopoly Oxometalates, Springer-Verlag, Berlin Heidelberg New York Tokyo, 1983.
[10] Y. Jeannin, J.P. Launay, M.A.S. Sedjadi, Inorg. Chem. 19 (1980) 2933–2935.
[11] P.P. Prosini, M. Lisi, D. Zane, M. Pasquali, Solid State Ionics 148 (2002) 45–51.
[12] Z. Bakenov, I. Taniguchi, J. Power Sources 195 (2010) 7445–7451.
[13] S. Manikumari, V. Shivaiah, S.K. Das, Inorg. Chem. 41 (2002) 6953–6955.
[14] F. Izumi, The Rietverd Method, Oxford University, Oxford, 1993.
[15] F. Izumi, T. Ikeda, Mater. Sci. Forum 198 (2000) 321–324.
[16] S. Kuroda, N. Tobori, M. Sakuraba, Y. Sato, J. Power Sources 119–121 (2003) 924–928.
[17] J.Y. Song, H.H. Lee, Y.Y. Wang, C.C. Wan, J. Power Sources 111 (2002) 255–267.
[18] C. Martin, C. Lamonier, M. Fournier, O. Mentré, V. Harlé, D. Guillaume, E. Payen, Inorg. Chem. 43 (2004) 4636–4644.
[19] V. Balraj, K. Vidyasagar, Inorg. Chem. 38 (1999) 1394–1400.
[20] R. Ratheesh, G. Suresh, V.U. Nayar, J. Solid State Chem. 118 (1995) 341–356.